J Biomol NMR (2011) 51:235–243
DOI 10.1007/s10858-011-9530-4

ARTICLE

Extensive de novo solid-state NMR assignments of the 33 kDa C-terminal domain of the Ure2 prion

Birgit Habenstein · Christian Wasmer · Luc Bousset · Yannick Sourigues · Anne Schütz · Antoine Loquet · Beat H. Meier · Ronald Melki · Anja Böckmann

Received: 25 February 2011 / Accepted: 11 July 2011 / Published online: 31 July 2011

Abstract We present the de novo resonance assignments for the crystalline 33 kDa C-terminal domain of the Ure2 prion using an optimized set of five 3D solid-state NMR spectra. We obtained, using a single uniformly ^{13}C, ^{15}N labeled protein sample, sequential chemical-shift information for 74% of the N, Cα, Cβ triples, and for 80% of further side-chain resonances for these spin systems. We describe the procedures and protocols devised, and discuss possibilities and limitations of the assignment of this largest protein assigned today by solid-state NMR, and for which no solution-state NMR shifts were available. A comparison of the NMR chemical shifts with crystallographic data reveals that regions with high crystallographic B-factors are particularly difficult to assign. While the secondary structure elements derived from the chemical shift data correspond mainly to those present in the X-ray crystal structure, we detect an additional helical element and structural variability in the protein crystal, most probably originating from the different molecules in the asymmetric unit, with the observation of doubled resonances in several parts, including entire stretches, of the protein. Our results provide the point of departure towards an atomic-resolution structural analysis of the C-terminal Ure2p domain in the context of the full-length prion fibrils.

Keywords Prion · Solid-state NMR · Fibrils · Sequential assignment · Conformational heterogeneity

Electronic supplementary material The online version of this article (doi:10.1007/s10858-011-9530-4) contains supplementary material, which is available to authorized users.

B. Habenstein · A. Loquet · A. Böckmann (✉)
Institut de Biologie et Chimie des Protéines, UMR 5086 CNRS/ Université de Lyon 1, 7 passage du Vercors, 69367 Lyon, France
e-mail: a.bockmann@ibcp.fr

C. Wasmer
Harvard Medical School, Boston, MA 02115, USA

C. Wasmer · A. Schütz · B. H. Meier (✉)
Physical Chemistry, ETH Zurich, Wolfgang-Pauli-Strasse 10, 8093 Zurich, Switzerland
e-mail: beme@ethz.ch

L. Bousset · Y. Sourigues · R. Melki (✉)
Laboratoire d'Enzymologie et Biochimie Structurales, UPR 3082 CNRS, Avenue de la Terrasse, 91198 Gif-sur-Yvette, France
e-mail: melki@lebs.cnrs-gif.fr

Present Address:
A. Loquet
Max Planck Institute for Biophysical Chemistry, Am Fassberg 11, 37077 Göttingen, Germany

Introduction

Prion oligomeric species associated to disease recruit and imprint their intrinsic conformation to the non-pathologic form of the protein (Prusiner 1982). Although actively studied, the structural changes accompanying the oligomerization of prion proteins, the mechanisms of pathologic and non-pathologic prion interactions, the processes at the origin of prion formation and propagation and the link between these changes and disease are far from being understood. To identify the molecular events associated with these processes and to decipher the architectural properties of pathologic prion assemblies that make them unique in that they propagate, site-resolved information on the atomic level is required. Solid-state NMR is one of the most promising techniques to reveal conformational details of insoluble and non-crystalline molecular assemblies (Castellani et al. 2002; Lange et al. 2005; Ferguson et al. 2006; Wasmer et al. 2008;

Manolikas et al. 2008; Loquet et al. 2008; Van Melckebeke et al. 2010; Franks et al. 2008; Jaroniec et al. 2004; Iwata et al. 2006; Helmus et al. 2008; Petkova et al. 2002; Nielsen et al. 2009). Current work has shown that structural and dynamic characterization of fibrils, as well as atomic-resolution structures, can be obtained by this method.

The Ure2 prion studied here is a two-domain protein, with its N-terminal domain, critical for prion propagation, spanning residues 1-93, and its globular C-terminal domain spanning residues 94-354. The structure of the C-terminal domain was solved using X-ray crystallography, and reveals a fold similar to glutathione *S*-transferases (Bousset et al. 2001). The prion domain is unusually rich in Asn, Gln, Ser and Thr residues. We recently presented, based on high-resolution two-dimensional solid-state NMR spectra, a rough structural analysis of the Ure2 prion fibrils and the isolated globular C-terminal/N-terminal prion domains (Loquet et al. 2009). The data suggested that the C-terminal domain displays an equally well-defined, homogeneous structure when part of the full-length fibrils and in isolation (in crystalline form). The observation of well-resolved spectra of the protein in the context of the fibrils offers the exciting possibility for a site-specific characterization of the fibrils and—ultimately—for an atomic-resolution NMR structure. In order to do so, the NMR resonance sequential assignment of the protein is required and is presented in the following.

Although the size of the proteins that can be sequentially assigned by solid-state NMR is steadily increasing, Ure2p94-354 still presents a considerable challenge. Most assignments recorded in the literature concern proteins of around 100 residues (McDermott et al. 2000; Pintacuda et al. 2007; Siemer et al. 2006b; Pauli et al. 2001; Böckmann et al. 2003; Igumenova et al. 2004; Marulanda et al. 2005; Franks et al. 2005; Lange et al. 2005; Goldbourt et al. 2007; Schneider et al. 2008; Jehle et al. 2009), but larger systems have been assigned, often using selective labeling strategies and supported by the availability of solution chemical shifts (Higman et al. 2009; Sperling et al. 2010). Also, recently, optimized strategies based on a set of three-dimensional experiments which use highly efficient adiabatic transfer schemes (Schuetz et al. 2010 and references herein) have been developed for the sequential assignment of uniformly ^{15}N, ^{13}C labeled protein. They employ a suite of sensitivity-optimized 3D experiments: NCACB, N(CO)CACB and CAN(CO)CB for the backbone, and extensions, e.g. CCC and NCACX, for the side-chain assignment. These experiments mainly use, on the carbon side, Cα and/or Cβ resonances taking advantage of their good spectral dispersion. A proof of principle was demonstrated for the 25 kDa HET-s(1-227) protein, where equally solution NMR assignment was performed for guidance (Schuetz et al. 2010).

Here we demonstrate the extensive de novo sequential assignments of the globular domain of the Ure2 prion, performed, in the absence of well-resolved solution NMR spectra, using solid-state NMR spectra only. The construct Ure2p70-354 investigated here includes, for the sake of expression yield and stability, the additional amino acid residues 70-93 from the prion domain. We report here residue-specific information for 74% of the N, Cα, Cβ, and 80% of the side-chain carbons of these assigned residues. We observe that the non-assigned residues often feature a large crystallographic B-factor, indicating that assignments are not only limited by the size of the protein (and thus resonance overlap), but also by the flexibility in some parts of the protein, reducing signal/noise in the NMR spectra. Structural variations, probably between symmetrically non-equivalent protein molecules in the unit cell, are revealed for several residues in the Ure2p70-354 sample by peak doubling, with chemical-shift differences of up to 3 ppm.

Materials and methods

Protein expression and purification

The procedures for Ure2p70-354 expression and purification are described in Loquet et al. (2009).

Crystallization of Ure2p70-354

Ure2p70-354 crystals were generated as described (Bousset et al. 2001). The protein crystals were directly centrifuged into the rotor during 30 min at 85000×*g* (Böckmann et al. 2009).

Solid-state NMR spectroscopy

All spectra were recorded on a Bruker Avance II + 850 MHz spectrometer operating at a static field of 20 T. A 3.2 mm Bruker triple resonance MAS probe equipped with an LLC coil was used to reduce r.f. heating during the experiments. The spectra were recorded at sample temperatures of about 7°C, as determined by the water resonance (Böckmann et al. 2009). The pulse sequences were implemented as recently reported (Schuetz et al. 2010) and all experimental parameters are given in Table S2. The NCACB spectrum was internally referenced to DSS and all other spectra were subsequently referenced to an isolated resonance in this spectrum. All spectra were processed in TopSpin 2.0 (Bruker Biospin) by zero filling to a power of two not larger than twice the number of points measured, apodizing with a cosine square function, Fourier transform followed by a polynomial baseline correction for the direct dimension. Spectra were analyzed and annotated using

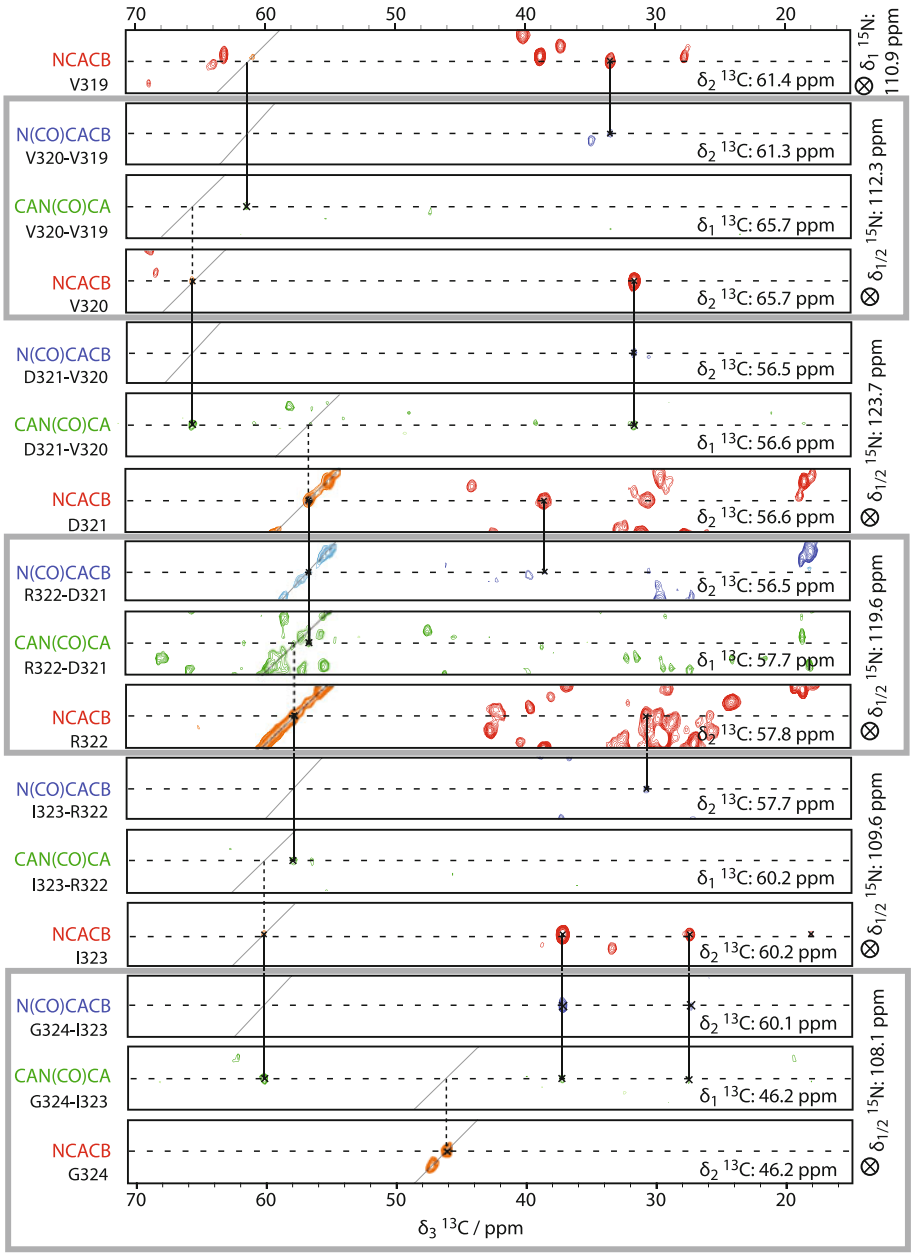

Fig. 1 Strip plot from three different 3D experiments showing the sequential walk for the amino acid stretch Val320–Gly324. *Solid lines* represent the assignments used in the sequential walk, and include, when observed, side-chain resonances. *Vertical dashed lines* indicate conserved Cα frequencies in two dimensions. *Grey frames* indicate the same ^{15}N frequency, however for different dimensions (δ_1 for NCACB, N(CO)CACB and δ_2 for CAN(CO)CA)

CCPNmr Analysis (Vranken et al. 2005). Protein structures were created using the program VMD (Humphrey et al. 1996).

Results and discussion

Sequential assignments

A sequential walk along the backbone resonances was carried out using a combination of 3D NCACB, N(CO)CACB and CAN(CO)CA spectra, as detailed previously (Schuetz et al. 2010). A strip-plot showing the assignment procedure for a five-amino-acid stretch is presented in Fig. 1. The strategy (summarized in Fig. 2a) is based on the principle that a cross-peak in the 3D spectrum correlates the resonance frequencies of three connected spins, of which two have been identified in the previous step and are now complemented by a new frequency, thereby extending the assignment to a further spin.

For several amino acids which exhibit a high signal-to-noise ratio, the CAN(CO)CA spectrum shows also Cβ resonances—arising from relayed transfers—and this information can complement the information of the N(CO)CACB spectrum, which is the least sensitive spectrum of the suite of experiments employed here. About 50% of the Ure2p70-354N, Cα, Cβ triples could be assigned using exclusively the strategy of Fig. 2a. For the

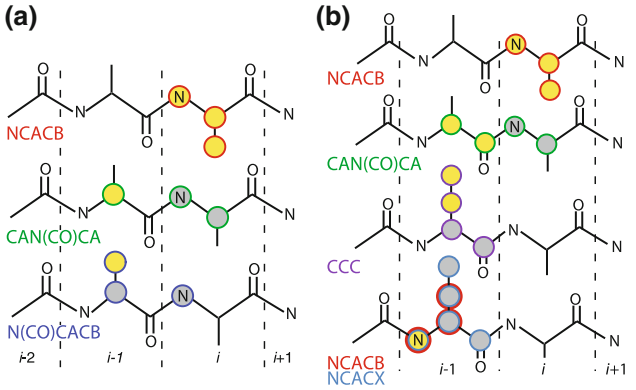

Fig. 2 **a** Assignment strategy presented in reference (Schuetz et al. 2010). **b** Extended assignment strategy. Resonance assignments provided by the considered assignment step are *yellow*, known resonances from the previous step are *grey*. Both strategies are possible in both directions

remaining triples, low signal to noise in the N(CO)CACB restricted completion of the walk.

In order to extend the assignments, we used a strategy involving additional 3D CCC and NCACX spectra as presented in Fig. 2b. The strategy relies on the use of N, C′, $C\alpha_i$ and side chain resonances: Starting from the N and Cα resonances of an assigned N_i, $C\alpha_i$, $C\beta_i$ frequency triple (from the NCACB spectrum) not only the $C\alpha_{i-1}$, but also the C'_{i-1} resonances can be identified in the CAN(CO)CA spectrum, since the C′ to Cα transfer is only partial. The $C\alpha_{i-1}$, C'_{i-1} pairs are, however, often assigned only in an ambiguous manner, as the 3D spectrum contains no C′/Cα correlations. Ambiguities at this stage can often be resolved by using the Cα, C′ resonances in the CCC experiment: from the C′ and Cα, the Cβ and possibly further side chain resonances can be identified. From this information and the combined use of the NCACB and the NCACX, which shows further side chain resonances and the C′ resonances, the N_{i-1} can be identified. The procedure is difficult using the NCACX without the NCACB, since the signal to noise is lower in the NCACX as compared to the NCACB. Also, the NCACX shows numerous inter-residue cross peaks that may complicate the unambiguous identification of the N_{i-1} $C\alpha_{i-1}$ $C\beta_{i-1}$ triple.

Ambiguities can often be resolved by information on the amino-acid type from the side-chain peaks in the CCC and NCACX spectra, or by progressing to residue i ± 2. A strip plot representing a sequential walk using this strategy is shown in Fig. 3.

Using the five 3D spectra, we could sequentially assign 74% of the N, Cα and Cβ resonances of residues 94-354. All assigned residues are colored in red on the tertiary (Bousset et al. 2001) (Fig. 4a) and primary structure (Fig. 4d) of Ure2p94-354.

Unassigned regions often contain "difficult" residues whose spin system is restricted to Cα/Cβ in the aliphatic region, as Ala, Asn, Asp and aromatic residues. The completeness of the assignments also clearly correlates with the crystallographic B-factor (reflecting the mean-square displacement of the atoms (Halle 2002)). This can be rationalized by analyzing the peak volume in the NCACB spectrum as a function thereof, as plotted in Fig. 4b. The mean B-factor of Cα of chain C and D for the PDB entry 1G6W is 36 ± 13 $Å^2$ for the unassigned and 25 ± 9 $Å^2$ for the assigned residues. Figure 4b shows that, for Ure2p94-354, a large B-factor always corresponds to a small peak volume. This finding can be explained by the fact that the polarization-transfer steps in all experiments become less efficient in the presence of molecular motion on the millisecond or faster timescale. Note however that the inverse is not true, as some of the spin systems with low B factors are still difficult to assign due to residual overlap, and "difficult" spin systems that have no aliphatic side chains. The experiments that include a (CO) step generally suffer more from weak SNR. The detailed intensity may also depend on the topology of the spin system and carrier-frequency dependence of the DREAM transfer (Schuetz et al. 2010). As small peak volumes result in increased

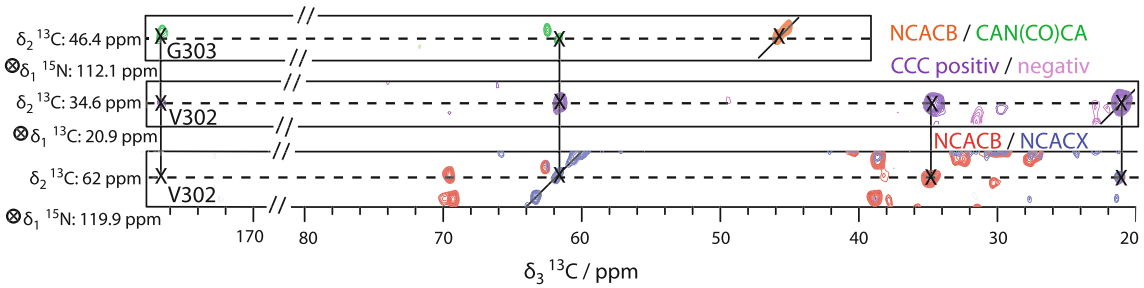

Fig. 3 Two-residue strip *plot* using the assignment procedures given in Fig. 2. *First strip*: overlay of NCACB (*red*) and CAN(CO)CA (*green*), identification of the N, Cα and Cβ resonances of residue i and of the potential C′ and Cα pair of residue i−1; *second strip*: CCC DREAM/PDSD (*purple*), verification of the C′ and Cα pair and identification of the potential corresponding side-chains of residue i−1; *third strip*: overlay of NCACB (*red* for negative, *orange* for positive contours) and NCACX (*blue*), identification of the corresponding residue i−1N frequency

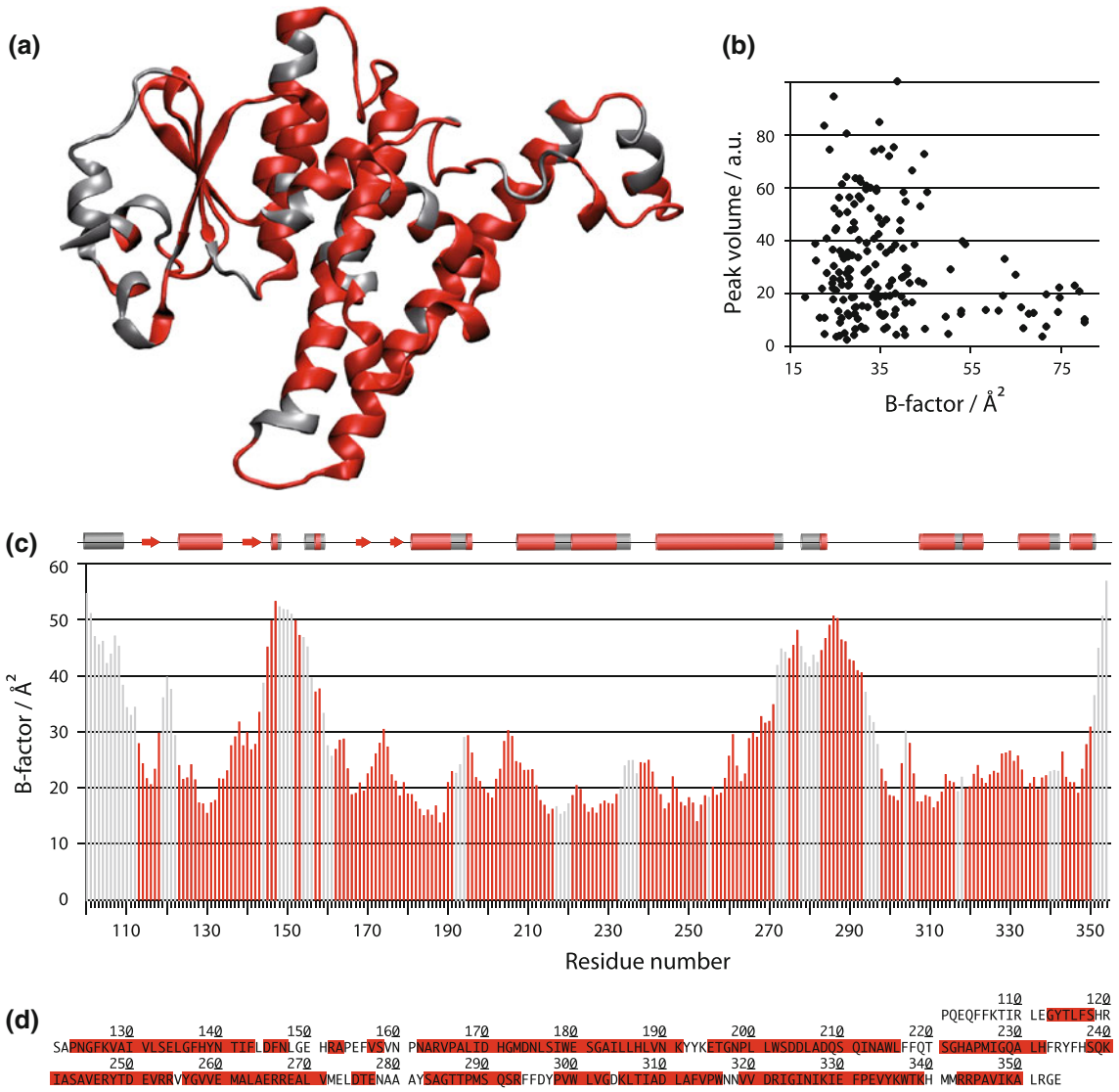

Fig. 4 **a** Crystal structure of Ure2p94-354 (PDB 1G6W chain C). Residues whose backbone resonances are assigned are colored in *red*. **b** *Plot* of the peak volumes of the N, Cα, Cβ cross peaks in the NCACB spectrum of the Ure2p C-terminal domain versus the crystallographic B-factor (of the Cα atom in PDB file 1G6Y, chain A) **c** Assigned residues (*red*) *plotted* on the structural motifs of 1G6Y and versus the B-factor (mean value of Cα for chains C and D, 1G6W). Unassigned residues are shown in *grey*. **d** Assignments shown on the primary structure

difficulties for sequential assignments, the assignment is often most incomplete in regions with high B-factors, as shown in Fig. 4c for residues 100-354 that are visible in the crystal structure. For a comparison of the assignment strategies and the B-factor on the structure, both are shown in Figure S1a (PDB entry 1G6W). For regions with high B-factors, sequential assignments using the more sensitive NCACB, CAN(CO)CA, CCC and NCACX spectra, providing all (N, C$'$, Cα_i and side chain) resonances, had to be used rather than the strategy requiring the well-resolved, but least sensitive N(CO)CACB measurements (Schuetz et al. 2010) (Figure S1b). The residues assigned using the strategy shown in Fig. 2a feature a mean B-factor of 22 $\pm$ 5 Å^2, while the strategy shown in Fig. 2b allowed the assignment for residues with a mean B-factor of 30 $\pm$ 12 Å^2. We find a similar correlation between the B-factor and the completeness of solid-state NMR assignments for HET-s(1-227) (Schuetz et al. 2010), as indicated in Figure S2. The line-width in the direct dimension (δ_3) in the 3D NCACB is, however, not correlated with the B-factor, suggesting that dynamic rather than static disorder, with a concomitant loss of polarization-transfer efficiency, is at the origin of the observed signal attenuation. The signal-to-noise ratio could be improved by increasing the signal averaging times, however, a factor of 2 in SNR leads already to impractically long measurement times of about 20 days for the least sensitive experiments, underlining the need for the development of more efficient

polarization-transfer steps or hyperpolarization techniques for studying even larger proteins.

Sequence-specific assignments were not achieved for 52(N, Cα, Cβ) triples (each corresponding to one spin system) in the NCACB spectrum, which could not be connected sequentially since the required spectra show an insufficient signal-to-noise ratio. Of these 52 peaks, 32 could be assigned in an amino-acid specific manner (see Figure S3) by a combined use of NCACB/NCACX and CCC spectra. The 20 remaining peaks are unlikely to originate from the 24 additional N-terminal amino-acids from the prion domain (vide supra) given their intensity and the abundance of the amino acid residues within this stretch (one Ala, Leu, Lys, Phe, Pro, Ser, and no Pro, Val, Met, Tyr). In addition, a J-coupling based INEPT spectrum (Andronesi et al. 2005; Andronesi et al. 2008; Siemer et al. 2006a) which is sensitive to flexible residues, shows peaks for all amino-acid types present in this additional stretch, notably the specific Hβ-Cβ resonances arising from the abundant Gln and Asn residues (Loquet et al. 2009). Thus, there is strong indication that many, if not all unassigned resonances in the CP-based spectra originate from the polypeptide chain spanning residues 94-354. The 24N-terminal residues from the prion domain are most likely not observable in these spectra, but are visible in the INEPT spectrum. This is consistent with the findings that this moiety of Ure2p is flexible (Thual et al. 2001, 1999) and disordered when the protein is in its native (soluble) state (Pierce et al. 2005). If one assumes that all the additionally visible but not sequentially assigned peaks originate from the C-terminal domain, 93% of the residues (243 out of 261) of Ure2p94-354 are visible in the NCACB spectrum of Ure2p70-354. Overall, 57% of all ^{13}C, ^{15}N resonances expected for residues 94-354 were assigned. It is interesting to note that signal overlap does not seem to be the major source for the incomplete assignment, but rather the insufficient signal-to-noise ratio in the dynamic parts of the molecule.

The extent of assignment could possibly be increased by combining the results from several selectively labeled samples (for an example see Higman et al. 2009) and/or additional experiments. A higher degree of assignment (85 vs. 74% here) was reported for DsbA recently (Sperling et al. 2010), and additional experiment types were performed in this study. However, many of them take a very long measurement time already for the smaller system of DsbA (229 amino-acid residues) and were therefore not considered for Ure2p where we concentrate on experiments with as many adiabatic polarization-transfer steps as possible.

A comparison between the chemical-shift predictions from the crystal structure using the Sparta program (Shen and Bax 2007) and the experimentally assigned chemical shifts shows a mean RMSD of 1.4 ppm for Cα, 1.3 ppm for Cβ and 3.5 ppm for N. There is no significant correlation within a given residue between the prediction accuracy for the Cα, Cβ or N shift, i.e. a correct prediction of one chemical shift of a given resonance does not imply the correct prediction of the other two. Figure S4 shows the chemical-shift deviation of the Sparta predictions from the assigned chemical shifts along the sequence. The chemical-shift predictions are of insufficient accuracy to be of direct use in the assignment process, but they can be used throughout the sequential assignment of carbon resonances to suggest a pathway in case of ambiguities, as can also secondary chemical shifts (Wang and Jardetzky 2002) or amino-acid typical chemical shifts (Ulrich et al. 2008). It goes without saying that these choices must be confirmed in the further course of the assignments.

Secondary chemical shift analysis

Figure 5 shows the secondary chemical shifts, i.e. the difference between the chemical-shift deviations of the observed Cα and Cβ shifts from the random coil shift (ΔδCα–ΔδCβ), as a function of the residue number along with the secondary structure elements observed in the X-ray structure (Bousset et al. 2001). These shifts are indicative of secondary structure elements: negative differences for more than three residues with a

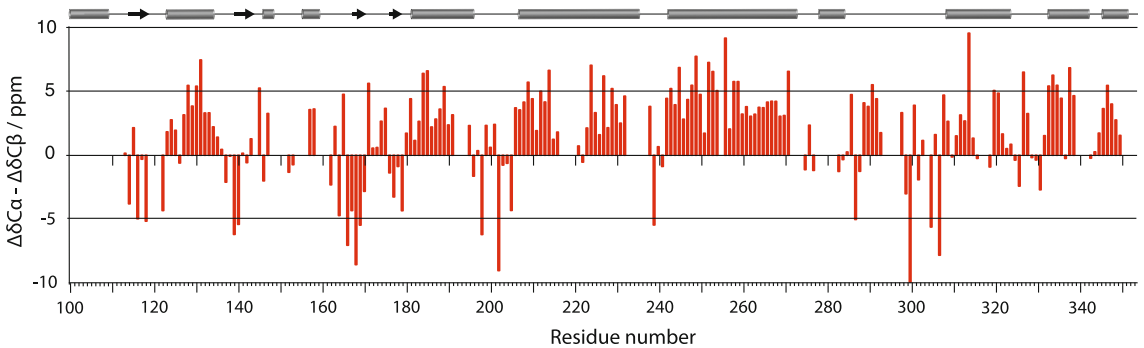

Fig. 5 Secondary chemical shift compared to the secondary structure from the crystal structure shown on the *top* (Bousset et al. 2001)

($\Delta\delta C\alpha - \Delta\delta C\beta$) $\leq$ 1.4 ppm imply a β-sheet secondary structure motif, and positive differences for more than four residues with a ($\Delta\delta C\alpha - \Delta\delta C\beta$) $\geq$ 1.4 ppm an α-helical arrangement (Spera and Bax 1991; Wishart et al. 1991; Wishart and Sykes 1994). The resulting structural motifs are consistent with the crystal structure for all residues. The resulting structural motifs are overall consistent with the crystal structure. The negative secondary chemical shift in the middle of the long helix spanning residues 207-237 well reflects the kink present in this helix. The five-in-a-row positive values for residues 288-292 point to a possible additional helix in this poorly defined part of the crystal structure.

Peak doubling is observed for several residues

Multiple peaks are identified for 7 residues, the amino-acid stretches 167-168 and 196-200 and for Ile178, within Ure2p94-354. Ala167–Leu168 and Ile178 show two peaks for the Cβ resonances, with a separation of up to 1.3 ppm for Ala167. The four amino acids Thr196–Leu200 are doubled in Cα and Cβ resonances with a separation of up to 1 ppm in the Cα shift for Gly197 and Asn198, 0.3 ppm in the Cβ shift (Asn198) and a separation of nearly 3 ppm in the N shift (Gly197). The assignment of this stretch is shown in Figure S5. The resonance frequencies are listed in Table S1.

The peak doubling reveals a structural heterogeneity that originates most probably from conformational differences between Ure2p molecules within the asymmetric crystallographic unit which contains four Ure2p molecules, organized as two dimers. Indeed, the crystal contacts involving the amino-acid stretch 196-200 that links the two sub-domains of Ure2p94-354, are dissimilar. While residues 196-200 within molecule D are located at about 4 Å from residues 235-245 of molecule C from the neighbor asymmetric unit, residues 196-200 within molecule C of the same asymmetric unit are at about 14 Å from residues 235-245 of molecule D from the neighbor asymmetric unit, but at less than 5 Å from residues 348 and 342 of molecule D (Figure S6). We note that the different environments of residues 196-200 do not result in a conspicuous variation of the corresponding dihedral angles (often the key variable for NMR shifts) between the respective molecules. The dihedral angle differences of molecules C and D are plotted in Fig. 6a. In order to estimate the chemical-shift changes corresponding to the angular variations, we predicted the corresponding chemical shifts differences using the Sparta, ShiftX and Camshift programs. A limited number of Cα resonances are predicted to show differences above a threshold of about 1 ppm, which we defined experimentally to be clearly observable as two separate resonances (Fig. 6b, for other resonances see Figure S7). Most of the residues predicted to show doubled resonances do however not exhibit such a characteristic. Furthermore, no observable splitting was predicted for the regions where we observed doubled resonances. As neither the resolution of the X-ray structure nor the accuracy of chemical-shift predictions from dihedral angles are currently of a quality that allows a detailed comparison, we simply conclude at this point that NMR data has the power to reveal even small structural heterogeneities, which we however cannot

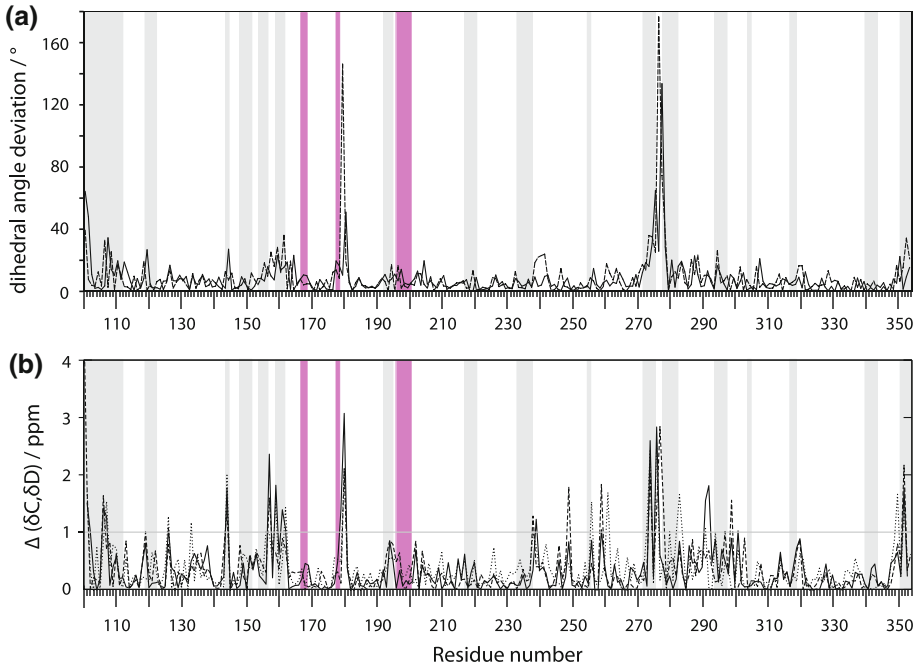

Fig. 6 **a** Variation of the Φ (*dotted*) and ψ (*continuous*) backbone angle differences between chains C and D as deposited in the PDB (entry 1G6W). Regions with *grey* background correspond to unassigned parts. *Pink background* highlights residues with observed peak doublings. **b** Differences between the Cα chemical shift predictions for chains C and D of 1G6W using Sparta (Shen and Bax 2007) (*solid line*), ShiftX (Neal et al. 2003) (*broken line*) and Camshift (Kohlhoff et al. 2009) (*dotted*). The *grey horizontal line* marks the threshold of 1 ppm above which differences should be readily observable in the NMR spectra

link directly to the dihedral angles deduced from the X-ray structure. Still, it seems clear that the observed doublings originate from slightly different conformations within the crystallographic unit, and possibly result from different contacts between the units (see Figure S6).

Conclusion

We here presented the extensive de novo sequential assignment of the crystalline globular C-terminal domain of the Ure2p prion spanning residues 94-354, with a molecular weight of 33 kDa, based on data from a single uniformly labeled sample. The set of five 3D spectra allowed us to assign 74% of the (N, Cα, Cβ) resonance triples, and 80% of the side chain resonances of the sequentially assigned residues. It proved important to also use side-chain and carbonyl resonance positions for the assignment. The assignment was predominantly limited by the signal-to-noise ratio of the spectra, which, in stretches with dynamic disorder as indicated by the high crystallographic B-factors tends to be lower and often, is insufficient for assignment. Of course, other factors like spectral crowding, the timescale of the dynamics underlying the B-factors, and the intrinsic properties of the spin systems also play an important role. It would be interesting to investigate the underlying dynamics of the backbone and sidechain motion but this is still a formidable task for a molecule of the size of Ure2p, and perdeuteration is needed for accurate results (Schanda et al. 2010, 2011). The signal overlap, in contrast, did not significantly limit the assignment in our case. This suggests that proteins that have molecular weight exceeding 33 kDa can be subjected to the assignment strategy we describe here. For proteins showing significant dynamics, signal-to-noise of the NMR experiments may further be improved by optimized polarization-transfer experiments, higher magnetic fields, or dynamic nuclear polarization techniques. Peak doubling is observed in our experiments for several residues, including a 5-amino-acid stretch, underlining the extraordinary sensitivity of NMR to conformational heterogeneity. As the C-terminal domain of the Ure2 prion is highly conserved in the context of the naturally occurring prion fibrils (Loquet et al. 2009), its sequential assignment presents the first step to a full structural characterization of Ure2 prion fibrils.

Acknowledgments This work was supported by the Agence Nationale de la Recherche (ANR-07-PCVI-0013-03, ANR-06-BLAN-0266, ANR-PCV08 321323, and ANR08-PCVI-0022-02), the ETH Zurich, the Swiss National Science Foundation (Grant 200020_124611) and the Centre National de la Recherche Scientifique. We also acknowledge support from the European Commission under the Seventh Framework Programme (FP7), contract Bio-NMR 261863.

References

Andronesi OC, Becker S, Seidel K, Heise H, Young HS, Baldus M (2005) Determination of membrane protein structure and dynamics by magic-angle-spinning solid-state NMR spectroscopy. J Am Chem Soc 127:12965–12974

Andronesi O, von Bergen M, Biernat J, Seidel K, Griesinger C, Mandelkow E, Baldus M (2008) Characterization of Alzheimer's-like paired helical filaments from the core domain of tau protein using solid-state NMR spectroscopy. J Am Chem Soc 130(130):5922–5928

Böckmann A, Lange A, Galinier A, Luca S, Giraud N, Juy M, Heise H, Montserret R, Penin F, Baldus M (2003) Solid-state NMR sequential resonance assignments and conformational analysis of the 2 × 10.4 kDa dimeric form of the Bacillus subtilis protein Crh. J Biomol NMR 27:323–339

Böckmann A, Gardiennet C, Verel R, Hunkeler A, Loquet A, Pintacuda G, Emsley L, Meier BH, Lesage A (2009) Characterization of different water pools in solid-state NMR protein samples. J Biomol NMR 45(3):319–327

Bousset L, Belrhali H, Janin J, Melki R, Morera S (2001) Structure of the globular region of the prion protein Ure2 from the yeast *Saccharomyces cerevisiae*. Structure 9(1):39–46

Castellani F, van Rossum B, Diehl A, Schubert M, Rehbein K, Oschkinat H (2002) Structure of a protein determined by solid-state magic-angle-spinning NMR spectroscopy. Nature 420:98–102

Ferguson N, Becker J, Tidow H, Tremmel S, Sharpe TD, Krause G, Flinders J, Petrovich M, Berriman J, Oschkinat H, Fersht AR (2006) General structural motifs of amyloid protofilaments. Proc Natl Acad Sci U S A 103(44):16248–16253

Franks WT, Zhou DH, Wylie BJ, Money BG, Graesser DT, Frericks HL, Sahota G, Rienstra CM (2005) Magic-angle spinning solid-state NMR spectroscopy of the beta1 immunoglobulin binding domain of protein G (GB1): 15N and 13C chemical shift assignments and conformational analysis. J Am Chem Soc 127(35):12291–12305

Franks WT, Wylie BJ, Schmidt HL, Nieuwkoop AJ, Mayrhofer RM, Shah GJ, Graesser DT, Rienstra CM (2008) Dipole tensor-based atomic-resolution structure determination of a nanocrystalline protein by solid-state NMR. Proc Natl Acad Sci USA 105(12):4621–4626

Goldbourt A, Day LA, McDermott AE (2007) Assignment of congested NMR spectra: carbonyl backbone enrichment via the Entner-Doudoroff pathway. J Magn Reson 189(2):157–165

Halle B (2002) Flexibility and packing in proteins. Proc Natl Acad Sci USA 99(3):1274–1279

Helmus JJ, Surewicz K, Nadaud PS, Surewicz WK, Jaroniec CP (2008) Molecular conformation and dynamics of the Y145Stop variant of human prion protein in amyloid fibrils. Proc Natl Acad Sci USA 105(17):6284–6289

Higman VA, Flinders J, Hiller M, Jehle S, Markovic S, Fiedler S, van Rossum BJ, Oschkinat H (2009) Assigning large proteins in the solid state: a MAS NMR resonance assignment strategy using selectively and extensively 13C-labelled proteins. J Biomol NMR 44(4):245–260

Humphrey W, Dalke A, Schulten K (1996) VMD—Visual molecular dynamics. J Molec Graphics 14(1):33–38

Igumenova TI, Wand AJ, McDermott AE (2004) Assignment of the backbone resonances for microcrystalline ubiquitin. J Am Chem Soc 126(16):5323–5331

Iwata K, Fujiwara T, Matsuki Y, Akutsu H, Takahashi S, Naiki H, Goto Y (2006) 3D structure of amyloid protofilaments of beta2-microglobulin fragment probed by solid-state NMR. Proc Natl Acad Sci USA 103(48):18119–18124

Jaroniec CP, MacPhee CE, Bajaj VS, McMahon MT, Dobson CM, Griffin RG (2004) High-resolution molecular structure of a peptide in an amyloid fibril determined by magic angle spinning NMR spectroscopy. Proc Natl Acad Sci U S A 101(3):711–716

Jehle S, van Rossum B, Stout JR, Noguchi SM, Falber K, Rehbein K, Oschkinat H, Klevit RE, Rajagopal P (2009) alphaB-crystallin: a hybrid solid-state/solution-state NMR investigation reveals structural aspects of the heterogeneous oligomer. J Mol Biol 385(5):1481–1497

Kohlhoff KJ, Robustelli P, Cavalli A, Salvatella X, Vendruscolo M (2009) Fast and accurate predictions of protein NMR chemical shifts from interatomic distances. J Am Chem Soc 131(39): 13894–13895

Lange A, Becker S, Seidel K, Giller K, Pongs O, Baldus M (2005) A concept for rapid protein-structure determination by solid-state NMR spectroscopy. Angew Chem Int Ed 44:2–5

Loquet A, Bardiaux B, Gardiennet C, Blanchet C, Baldus M, Nilges M, Malliavin T, Boeckmann A (2008) 3D structure determination of the Crh protein from highly ambiguous solid-state NMR restraints. J Am Chem Soc 130(11):3579–3589

Loquet A, Bousset L, Gardiennet C, Sourigues Y, Wasmer C, Habenstein B, Schütz A, Meier BH, Melki R, Böckmann A (2009) Prion fibrils of Ure2p assembled under physiological conditions contain highly ordered, natively folded modules. J Mol Biol 394:108–118

Manolikas T, Herrmann T, Meier BH (2008) Protein structure determination from 13C Spin-diffusion solid-state. NMR J Am Chem Soc 130(12):3959–3966

Marulanda D, Tasayco ML, Cataldi M, Arriaran V, Polenova T (2005) Resonance assignments and secondary structure analysis of *E. coli* thioredoxin by magic angle spinning solid-state NMR spectroscopy. J Phys Chem B (109):18135–18145

McDermott A, Polenova T, Böckmann A, Zilm KW, Paulsen EK, Martin RW, Montelione GT (2000) Partial NMR assignments for uniformly (13C, 15N)-enriched BPTI in the solid state. J Biomol NMR 16:209–219

Neal S, Nip AM, Zhang H, Wishart DS (2003) Rapid and accurate calculation of protein 1H, 13C and 15N chemical shifts. J Biomol NMR 26(3):215–240

Nielsen JT, Bjerring M, Jeppesen MD, Pedersen RO, Pedersen JM, Hein KL, Vosegaard T, Skrydstrup T, Otzen DE, Nielsen NC (2009) Unique identification of supramolecular structures in amyloid fibrils by solid-state NMR spectroscopy. Angew Chem Int Ed 48(12):2118–2121

Pauli J, Baldus M, van Rossum B, de Groot H, Oschkinat H (2001) Backbone and side-chain C-13 and N-15 signal assignments of the alpha-spectrin SH3 domain by magic angle spinning solid-state NMR at 17.6 tesla. Chembiochem 2(4):272–281

Petkova AT, Ishii Y, Balbach JJ, Antzutkin ON, Leapman RD, Delaglio F, Tycko R (2002) A structural model for Alzheimer's beta -amyloid fibrils based on experimental constraints from solid state NMR. Proc Natl Acad Sci USA 99(26):16742–16747

Pierce MM, Baxa U, Steven AC, Bax A, Wickner RB (2005) Is the prion domain of soluble Ure2p unstructured? Biochemistry 44(1):321–328

Pintacuda G, Giraud N, Pierattelli R, Bockmann A, Bertini I, Emsley L (2007) Solid-state NMR spectroscopy of a paramagnetic protein: assignment and study of human dimeric oxidized CuII-ZnII superoxide dismutase (SOD). Angew Chem Int Ed 46(7): 1079–1082

Prusiner SB (1982) Novel proteinaceous infectious particles cause scrapie. Science 216:136–144

Schanda P, Meier BH, Ernst M (2010) Quantitative analysis of protein backbone dynamics in microcrystalline ubiquitin by solid-state NMR spectroscopy. J Am Chem Soc 132(45):15957–15967

Schanda P, Meier BH, Ernst M (2011) Accurate measurement of one-bond H-X heteronuclear dipolar couplings in MAS solid-state NMR. J Magn Reson 210(2):246–259

Schneider R, Ader C, Lange A, Giller K, Hornig S, Pongs O, Becker S, Baldus M (2008) Solid-state NMR spectroscopy applied to a chimeric potassium channel in lipid bilayers. J Am Chem Soc 130(23):7427–7435

Schuetz A, Wasmer C, Habenstein B, Verel R, Greenwald J, Riek R, Böckmann A, Meier BH (2010) Protocols for the sequential solid-state NMR spectroscopic assignment of a uniformly labeled 25 kDa protein: HET-s(1–227). ChemBioChem 11(11): 1543–1551

Shen Y, Bax A (2007) Protein backbone chemical shifts predicted from searching a database for torsion angle and sequence homology. J Biomol NMR 38(4):289–302

Siemer AB, Arnold AA, Ritter C, Westfeld T, Ernst M, Riek R, Meier BH (2006a) Observation of highly flexible residues in amyloid fibrils of the HET-s prion. J Am Chem Soc 128(40): 13224–13228

Siemer AB, Ritter C, Steinmetz MO, Ernst M, Riek R, Meier BH (2006b) 13C, 15N resonance assignment of parts of the HET-s prion protein in its amyloid form. J Biomol NMR 34(2):75–87

Spera S, Bax A (1991) Empirical correlation between protein backbone conformation and Cα and Cβ ^{13}C nuclaer magnetic resonance chemical shifts. J Am Chem Soc 113:5490–5492

Sperling LJ, Berthold DA, Sasser TL, Jeisy-Scott V, Rienstra CM (2010) Assignment strategies for large proteins by magic-angle spinning NMR: the 21-kDa disulfide-bond-forming enzyme DsbA. J Mol Biol 399(2):268–282

Thual C, Komar AA, Bousset L, Fernandez-Bellot E, Cullin C, Melki R (1999) Structural characterization of *Saccharomyces cerevisiae* prion-like protein Ure2. J Biol Chem 274(19):13666–13674

Thual C, Bousset L, Komar AA, Walter S, Buchner J, Cullin C, Melki R (2001) Stability, folding, dimerization, and assembly properties of the yeast prion Ure2p. Biochemistry 40(6):1764–1773

Ulrich EL, Akutsu H, Doreleijers JF, Harano Y, Ioannidis YE, Lin J, Livny M, Mading S, Maziuk D, Miller Z, Nakatani E, Schulte CF, Tolmie DE, Kent Wenger R, Yao H, Markley JL (2008) BioMagResBank. Nucleic Acids Res 36(Database issue):D402–D408

Van Melckebeke H, Wasmer C, Lange A, Ab E, Loquet A, Böckmann A, Meier BH (2010) Atomic-resolution three-dimensional structure of HET-s(218-289) amyloid fibrils by solid-state NMR spectroscopy. J Am Chem Soc 132(39):13765–13775

Vranken WF, Boucher W, Stevens TJ, Fogh RH, Pajon A, Llinas M, Ulrich EL, Markley JL, Ionides J, Laue ED (2005) The CCPN data model for NMR spectroscopy: development of a software pipeline. Proteins 59(4):687–696

Wang YJ, Jardetzky O (2002) Probability-based protein secondary structure identification using combined NMR chemical-shift data. Protein Sci 11(4):852–861

Wasmer C, Lange A, Melckebeke HV, Siemer AB, Riek R, Meier BH (2008) Amyloid fibrils of the HET-s(218–289) prion form a beta solenoid with a triangular hydrophobic core. Science 319: 1523–1526

Wishart DS, Sykes BD (1994) The 13C chemical-shift index: a simple method for the identification of protein secondary structure using 13 chemical-shift data. J Biomol NMR 4:171–180

Wishart DS, Sykes BD, Richards FM (1991) Relationship between nuclear magnetic resonance chemical shift and protein secondary structure. J Mol Biol 222(2):311–333